Acta Crystallographica Section A
Foundations of Crystallography
ISSN 0108-7673

Received 6 February 2001
Accepted 16 April 2001

Diffraction by the ideal paracrystal

J. L. Eads and R. P. Millane*

Whistler Center for Carbohydrate Research, and Computational Science and Engineering Program, Purdue University, West Lafayette, Indiana 47907-1160, USA. Correspondence e-mail: rmillane@purdue.edu

A detailed analysis is made of the statistics and diffraction by a general, finite, two-dimensional ideal paracrystal. The statistics of the diagonal chain through the ideal paracrystal are derived, and the special cases of square and hexagonal ideal paracrystals are considered. Expressions for the diffraction are derived and characteristics of diffraction patterns are discussed in terms of the different parameters of the model for square and hexagonal ideal paracrystals. The variation of peak widths with scattering angle along different directions in reciprocal space is examined.

1. Introduction

Disordered crystalline materials are ubiquitous in nature and technology, and X-ray diffraction is an important means of analyzing such materials (Welberry, 1985; Stroud & Millane, 1995). Such analysis requires a statistical model of the disordered system and a method for calculating diffraction patterns based on the model. Models of crystalline disorder are therefore useful for both describing such materials and analyzing their diffraction data. One model that has been used to describe two- and three-dimensional disordered crystalline lattices is the ideal paracrystal. Properties and diffraction by the ideal paracrystal model are examined in detail in this paper.

Disordered crystalline systems can be conveniently described in terms of *lattice disorder* and *substitution disorder*. Substitution disorder consists of variations in the units (different atoms or molecules, or different orientations of the same molecule) located at each site of the crystal lattice. Lattice disorder consists of variations in the positions of the lattice sites away from those of an ordered periodic lattice. Substitution disorder generally induces some degree of lattice disorder, but we restrict ourselves here to lattice disorder (without considering the underlying basis for the disorder). The simplest kind of lattice disorder is referred to as thermal disorder, disorder of the *first kind* (Hosemann & Bagchi, 1962) or uncorrelated disorder (Stroud & Millane, 1996), which involves independent distortions of the lattice sites away from those of a regular periodic lattice. However, close-packed systems generally exhibit correlated disorder in which the distortions at neighboring sites are dependent. Correlated disorder can be characterized by examination of X-ray diffraction peak broadening with scattering angle. X-ray diffraction shows that correlated disorder is present in a variety of crystalline materials (Alexander, 1969; Hosemann & Hindeleh, 1995; Welberry & Butler, 1995).

Two principal models have been used to describe disordered crystalline materials, the paracrystal and the perturbed lattice, both of which incorporate correlated disorder. The paracrystal model was developed by Hosemann and coworkers (Hosemann & Bagchi, 1962) and has been widely used to analyze diffraction from disordered materials such as polymers, glasses and alloys (Hosemann & Hindeleh, 1995), and is based on a statistical description in terms of the lengths and directions of the nearest-neighbor intersite vectors in a distorted lattice. The perturbed lattice, on the other hand, describes a distorted lattice in terms of the displacements of its sites away from those of a periodic reference lattice (Welberry *et al.*, 1980; Welberry, 1985; Stroud & Millane, 1996). Both the paracrystal and the perturbed lattice models are well defined in one dimension but are well defined only under restricted conditions in more than one dimension (Welberry, 1985). In particular, in a two- or three-dimensional lattice, there are many more cell edges than lattice points, implying that conditional dependencies must be imposed on their distributions (Hammersley, 1967). An important result is that, at least in three dimensions, disordered lattices with stationary statistics have bounded variations away from an underlying regular lattice. The perturbed lattice model circumvents the difficulty with the cell edges by working with the lattice points themselves, rather than the vectors between them. The perturbed lattice describes a distorted lattice in terms of the correlated displacements of its sites away from those of a periodic reference lattice (Welberry & Carroll, 1982). Although there are still difficulties with constructing two- and three-dimensional perturbed lattices, the sites do have bounded deviations away from the underlying regular lattice and the perturbed lattice provides a rather general model of disorder. The reader interested in perturbed lattices is referred to the above references.

The one-dimensional paracrystal is a useful model for describing disorder in one-dimensional systems such as poly-

mers and for materials such as layered structures in which the disorder is one-dimensional (Egelman & DeRosier, 1982; Biswas & Blackwell, 1988; Hall & Somashekar, 1991; Mu *et al.*, 1997). The one-dimensional paracrystal model is easily extended to include thermal-like (uncorrelated) disorder and it is then similar to the one-dimensional perturbed lattice model (Millane & Eads, 2000). The one-dimensional paracrystal has been used to analyze higher-dimensional disorder by analysis of diffraction along particular directions in reciprocal space and interpretation in terms of the disorder in the corresponding planes in real space. However, this is not generally a satisfactory approach as it ignores the higher-dimensional character of the disorder. A proper analysis requires a model of higher-dimensional disorder.

A number of attempts have been made to extend the paracrystal model to higher dimensions (we consider here the two-dimensional case only). Such an extension is non-trivial however, since the statistics of the vectors joining neighboring lattice sites must be specified such that the vectors around the edges of each lattice cell close (Fig. 1). This appears not to be possible in general, and so various restricted or approximate models have been proposed. Each of these models has different drawbacks. The simplest model is to describe the two-dimensional distorted lattice as a set of independent parallel one-dimensional paracrystals (Baltá-Calleja & Hosemann, 1980). This model is generally unsatisfactory as it does not incorporate cumulative disorder in the orthogonal direction. Another simple model is the *ideal paracrystal* (Hosemann & Bagchi, 1962). The ideal paracrystal is constructed by generating two independent paracrystals along the two primary crystal axes and forming a two-dimensional distorted lattice from these. The disadvantages of this model are that the resulting cells of each distorted lattice are parallelograms (so that the disorder of the individual lattices is restricted), the disorder is anisotropic (in the sense that the disorder is different in the diagonal direction than in the axial directions), and it predicts excess low-angle diffraction (Perret & Ruland, 1971; Brämer & Ruland, 1976). In an attempt to reduce the degree of anisotropy in the ideal paracrystal model, Hosemann & Bagchi (1962) described the *real paracrystal* in which they included separate and independent distributions on the distances between the two pairs of diagonally opposite lattice sites of cells of the ideal paracrystal. However, Brämer & Ruland (1976) showed that this construction in fact constrains the lattice cells even more than for the case of the ideal paracrystal, and each lattice is actually periodic with the periodic unit consisting of two cells of the original lattice. This is not therefore a useful model of a disordered lattice. A similar approach has been used by Busson & Doucet (2000) to develop a hexagonal paracrystalline-like model in which the distribution function and the diffraction pattern have hexagonal symmetry. However, this model does not specify the statistics of the individual lattices, so that the validity of the model is not clear. Another attempt to generalize the paracrystal to two dimensions is the *spiral paracrystal* (Janke & Hosemann, 1978; Hosemann *et al.*, 1981; Eads & Millane, 2000). The spiral paracrystal is a somewhat *ad hoc* construction that involves packing a one-dimensional paracrystalline-like chain on itself in a spiral fashion. Although this is an interesting model, the statistics of the resulting lattices and their diffraction properties are not known and the model is not amenable to analytical analysis.

Among the two-dimensional paracrystalline models described above, the ideal paracrystal model has the advantage that its statistics are well defined and its diffraction pattern is easily calculated (for Gaussian statistics). The model has been applied to, for example, colloidal suspensions and block copolymer films (Matsuoka *et al.*, 1987), and polymer fibers (Granier *et al.*, 1989). Although all paracrystalline-type models in more than one dimension have limitations and short comings, they can be useful when used within their limitations. Since individual ideal paracrystalline lattices represent a restricted form of disorder, the model should not be interpreted in terms of the specific arrangements of units within a

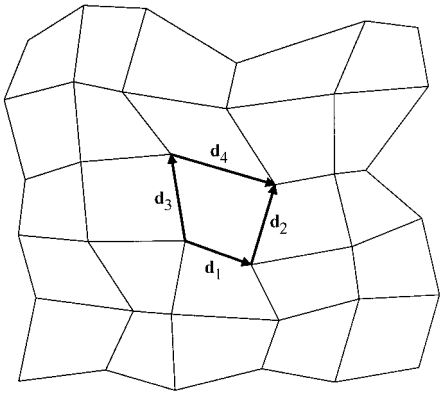

Figure 1
The cell closure constraint. The statistics of the intersite vectors must be specified such that $\mathbf{d}_1 + \mathbf{d}_2 = \mathbf{d}_3 + \mathbf{d}_4$.

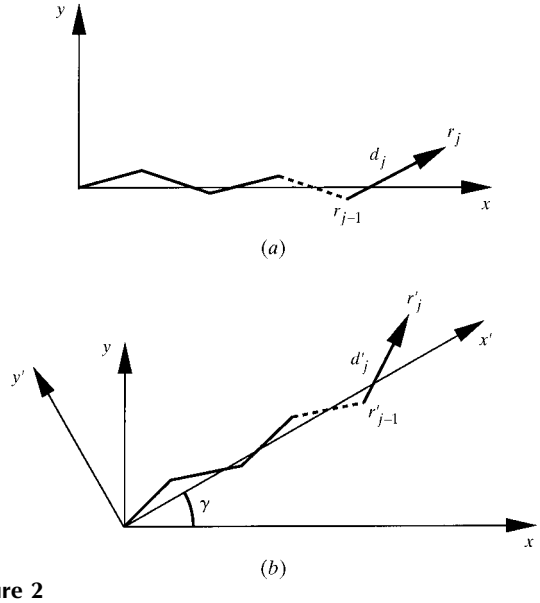

Figure 2
A one-dimensional paracrystal (*a*) along the *x* axis, and (*b*) inclined to the *x* axis.

disordered lattice, but rather in terms of an ensemble of such lattices, and the general character and degree of the disorder as derived from diffraction data. Furthermore, when one considers a finite lattice (*i.e.* the physically relevant case and the case considered here), the low-angle diffraction from the ideal paracrystal is well behaved (as is shown here).

There are few systematic studies of the characteristics of diffraction patterns from ideal paracrystals as a function of the various parameters of the model. Hosemann & Müller (1970) used optical diffraction to study the general characteristics of patterns from a variety of ideal paracrystalline arrays of points. Matsuoka *et al.* (1987) calculated the spherically averaged diffraction from cubic ideal paracrystals with various crystal symmetries. Furthermore, most discussion is in terms of an infinite ideal paracrystal, although it is well known that paracrystalline domains have a limited size (Hosemann *et al.*, 1981; Eads & Millane, 2000). Distortion parameters along particular directions in real space are often estimated by analysis of the variation of peak widths with scattering angle along the corresponding directions in reciprocal space using a one-dimensional model, whereas analysis in the context of a multidimensional model is required. We develop a general model of the finite ideal paracrystal and present a systematic study of its diffraction properties. The results are potentially useful in the interpretation of diffraction data from systems incorporating cumulative disorder.

The ideal paracrystal is described in detail in §2, and the special cases of square and hexagonal paracrystals considered. Diffraction by finite ideal paracrystals is derived in §3. Examples of diffraction patterns from finite square and hexagonal ideal paracrystals, for various values of the different parameters, are presented in §4 and peak broadening is studied in detail. Concluding remarks are made in §5.

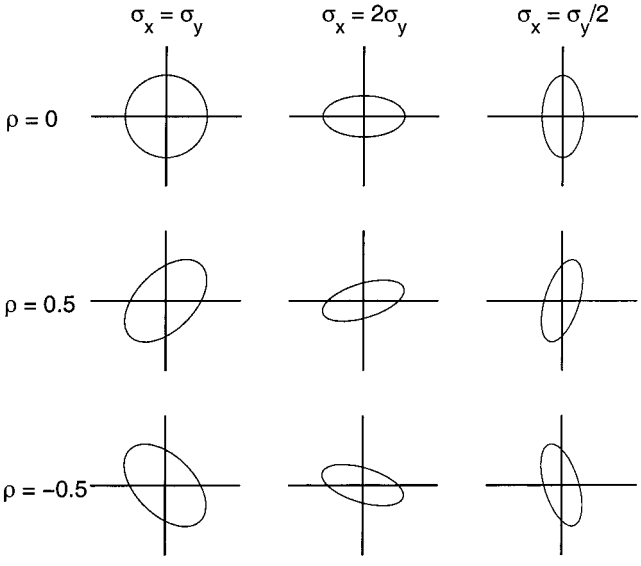

Figure 3
One contour level of the joint density $P(d^x - a, d^y)$ for the values of the parameters as shown.

2. The ideal paracrystal

The statistical properties of the two-dimensional ideal paracrystal are described in this section. Since the ideal paracrystal is most easily described in terms of two one-dimensional paracrystals in the plane, the one-dimensional paracrystal is described first.

2.1. The one-dimensional paracrystal

Consider a one-dimensional paracrystal in the plane, *i.e.* a linear periodic lattice that is distorted into two dimensions (Fig. 2*a*). The position of the jth site, $\mathbf{r}_j$, is then given by

$$\mathbf{r}_j = \mathbf{r}_{j-1} + \mathbf{d}_j = \sum_{k=1}^{j} \mathbf{d}_k, \tag{1}$$

where the $\mathbf{d}_j$ are random vectors and $\mathbf{r}_0 = \mathbf{d}_0 = \mathbf{0}$ (Fig. 2*a*). We consider a finite lattice with N lattice points so that $j = 0, 1, \ldots, N-1$. The Cartesian components of $\mathbf{d}_j$ are denoted by d_j^x and d_j^y. The mean axis of the paracrystal is taken to be the x axis, so that $\langle d^x \rangle = a$ and $\langle d^y \rangle = 0$, where a is the mean lattice spacing. The d_j^x and d_j^y are taken to be jointly normal, so that their joint density $P(d_j^x, d_j^y)$ is

$$P(d^x, d^y) = [2\pi\sigma_x\sigma_y(1-\rho^2)^{1/2}]^{-1} \times \exp\left(-\frac{1}{2(1-\rho^2)}\left[\frac{(d^x-a)^2}{\sigma_x^2} - 2\rho\frac{(d^x-a)d^y}{\sigma_x\sigma_y} + \frac{(d^y)^2}{\sigma_y^2}\right]\right), \tag{2}$$

where σ_x^2 and σ_y^2 are the variances of d^x and d^y, respectively, and $\rho = (\langle d^x d^y \rangle - \langle d^x \rangle\langle d^y \rangle)/\sigma_x\sigma_y$ is the correlation coefficient between d^x and d^y. As a matter of convenience, the covariance $C = (\langle d^x d^y \rangle - \langle d^x \rangle\langle d^y \rangle)$ (rather than the correlation coefficient) will often be used in this paper. The correlation coefficient is easily calculated from C as $\rho = C/\sigma_x\sigma_y$.

The characteristics of a paracrystal are controlled by the parameters σ_x, σ_y and ρ, and their effects are illustrated in Fig. 3, which shows one contour level of $P(d^x - a, d^y)$ for various values. If d^x and d^y are uncorrelated ($\rho = 0$), the aspect ratio of the probability ellipse is determined by σ_x/σ_y. If d^x and d^y are correlated ($\rho \neq 0$), the orientation of the major axis, and the aspect ratio, of the ellipse are determined by both σ_x/σ_y and ρ. The limiting orientation of the ellipse as $\rho \rightarrow \pm 1$ is determined by σ_x/σ_y. The distribution in a particular crystalline material will depend on the lattice system and the shapes and interactions of the particular molecules.

It is convenient to consider a one-dimensional paracrystal rotated relative to the coordinate system (Fig. 2*b*). The paracrystal lies along the x' axis, the (x', y') coordinate system being rotated by γ relative to the (x, y) coordinate system. The statistics of the intersite vectors $\mathbf{d}'_j = (d_j^{x'}, d_j^{y'})$ in the (x', y') coordinate system are as described above and with parameters $\langle d^{x'} \rangle = a$, $\langle d^{y'} \rangle = 0$, $\sigma_{x'}^2$, $\sigma_{y'}^2$ and ρ'. We denote by $\mathbf{d}_j = (d_j^x, d_j^y)$ the vector $\mathbf{d}'_j$ in the (x, y) coordinate system. Since the d_j^x and d_j^y are linear functions of the $d_j^{x'}$ and $d_j^{y'}$, they are also jointly normal, and using the appropriate coordinate transformation shows that the statistics of d_j^x and d_j^y are described by

$$\langle d^x \rangle = a \cos\gamma \tag{3}$$

$$\langle d^y \rangle = a \sin\gamma \tag{4}$$

$$\sigma_x^2 = \sigma_{x'}^2 \cos^2\gamma + \sigma_{y'}^2 \sin^2\gamma - C' \sin 2\gamma \tag{5}$$

$$\sigma_y^2 = \sigma_{x'}^2 \sin^2\gamma + \sigma_{y'}^2 \cos^2\gamma + C' \sin 2\gamma \tag{6}$$

$$C = \tfrac{1}{2}(\sigma_{x'}^2 - \sigma_{y'}^2)\sin 2\gamma + C' \cos 2\gamma. \tag{7}$$

Note that d_j^x and d_j^y are uncorrelated only if the covariance of the inclined paracrystal satisfies

$$C' = \tfrac{1}{2}(\sigma_{y'}^2 - \sigma_{x'}^2)\tan 2\gamma. \tag{8}$$

Note also that this is the case if the components of the distortions of the inclined paracrystal are uncorrelated ($C' = 0$) and have equal variances ($\sigma_{x'} = \sigma_{y'}$). Also, in this case, referring to (5) and (6), $\sigma_x = \sigma_y = \sigma_{x'} = \sigma_{y'}$.

2.2. The ideal paracrystal

Consider two one-dimensional paracrystals in the plane, one oriented along the x axis and one orientated at an angle γ to the x axis, and denote the average lattice vectors by **a** and **b**, respectively (Fig. 4*a*). The variances of the paracrystal along the a axis, parallel and normal to its axis, are denoted by σ_a and $\sigma_{a\perp}$, respectively, and the covariance by C_a. The same parameters along the b axis are denoted by σ_b, $\sigma_{b\perp}$ and C_b. Let the position vectors of the lattice points of the two one-dimensional paracrystals be denoted by $\mathbf{s}_j$ and $\mathbf{t}_k$. The ideal paracrystal is defined as follows. The position $\mathbf{r}_{jk}$ of the (j, k)th site of the ideal paracrystal is given by

$$\mathbf{r}_{jk} = \mathbf{s}_j + \mathbf{t}_k. \tag{9}$$

This leads to the construction shown in Fig. 4(*a*) and the paracrystalline lattice is made up of parallelograms whose edges are defined by the component one-dimensional paracrystals. We assume that the intersite vectors of the two one-dimensional paracrystals are uncorrelated with each other. The construction based on two one-dimensional paracrystals restricts the kinds of disorder that can be represented, but it does ensure cell closure.

The ideal paracrystal can be described as the convolution of two one-dimensional paracrystals. In order to demonstrate this, it is convenient to describe a lattice by a function $f(x, y)$ that is a periodic array of δ functions. The two one-dimensional paracrystals shown in Fig. 4(*a*), denoted by $f_a(x, y)$ and $f_b(x, y)$, are then represented as

$$\begin{aligned} f_a(x, y) &= \sum_j \delta(x - s_j^x, y - s_j^y) \\ f_b(x, y) &= \sum_k \delta(x - t_k^x, y - t_k^y), \end{aligned} \tag{10}$$

where $\delta(x, y)$ is the two-dimensional Dirac δ function. The ideal paracrystal, denoted by $g(x, y)$, is then given by

$$\begin{aligned} g(x, y) &= \sum_j \sum_k \delta(x - r_{jk}^x, y - r_{jk}^y) \\ &= f_a(x, y) \otimes f_b(x, y), \end{aligned} \tag{11}$$

where $\otimes$ denotes convolution. Note that in (11) we have implicitly replaced $f_b(x, y)$ by $f_b(-x, -y)$, since the properties of the paracrystal are invariant to inversion in the origin. The convolutional property (11) is useful when describing diffraction by the ideal paracrystal.

Consider a chain of lattice sites embedded in an ideal paracrystal such that their indices (j, k) satisfy $iq = jp$, where p and q are any integer constants. This chain of sites forms a one-dimensional lattice, two examples of which, for $p = q = 1$ and $p = 2, q = 1$, are shown in Fig. 4(*b*). If the sites of this lattice are indexed by j, the coordinates of the sites, $\mathbf{w}_j$, are given by

$$\mathbf{w}_j = \mathbf{r}_{jp,jq}, \tag{12}$$

where $\mathbf{r}_{jk}$ are the coordinates of the sites of the underlying ideal paracrystalline lattice. The coordinates can be written as

$$\begin{aligned} \mathbf{w}_j &= \mathbf{w}_{j-1} + \left(\sum_{i=(j-1)p+1}^{jp} \mathbf{d}_i + \sum_{i=(j-1)q+1}^{jq} \mathbf{d}_i' \right) \\ &= \mathbf{w}_{j-1} + \mathbf{e}_j, \end{aligned} \tag{13}$$

where $\mathbf{d}_i$ and $\mathbf{d}_i'$ are the intersite vectors of the one-dimensional paracrystals that form the underlying ideal paracrystal. Since the $\mathbf{d}_i$ and $\mathbf{d}_i'$ are independent and normally distributed, the $\mathbf{e}_j$ are normally distributed. Comparing (1) and (13) shows that any such chain of sites is a one-dimensional paracrystal.

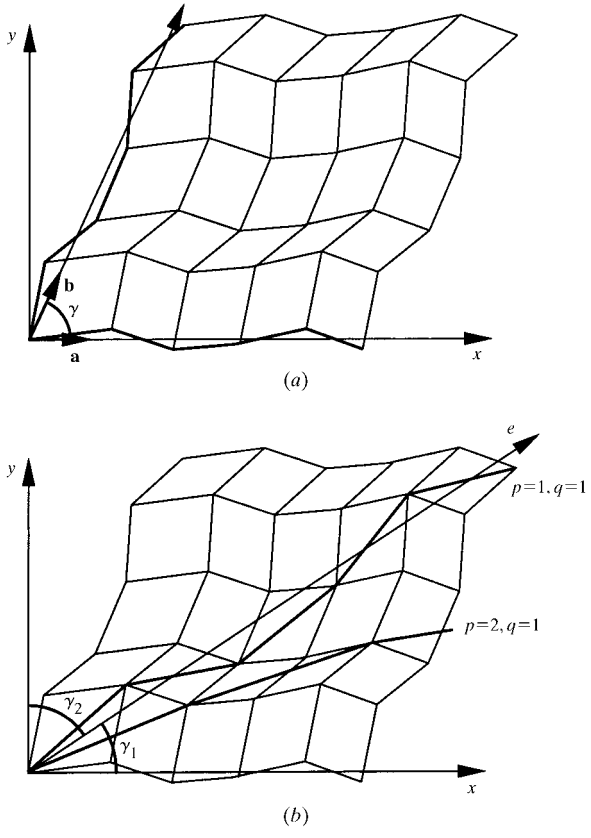

Figure 4
(*a*) The ideal paracrystal defined in terms of two one-dimensional paracrystals. (*b*) Two one-dimensional lattices through an ideal paracrystal for $p = 1, q = 1$ and $p = 2, q = 1$, as described in the text.

2.3. Statistics of diagonal neighbors

The structure of a disordered lattice is determined by the interactions of neighboring molecules. First nearest neighbors are generally at neighboring lattice sites along the primary axes, but neighbors across the cell diagonals [the (1, 1) direction] are also often close neighbors and their interactions may be significant in determining the structure of the disordered lattice. The statistics along this diagonal are therefore relevant. An intersite vector $\mathbf{e}_j$ along the diagonal paracrystal is given by

$$\mathbf{e}_j = \mathbf{d}_j + \mathbf{d}'_j, \tag{14}$$

where $\mathbf{d}_j$ and $\mathbf{d}'_j$ are the intersite vectors along **a** and **b**, respectively. The parameters describing the statistics of the $\mathbf{e}_j$ (in the Cartesian coordinate system for which one axis is coincident with the mean axis of the diagonal paracrystal) are denoted by σ_e, $\sigma_{e\perp}$ and C_e, and we wish to determine these parameters. The average spacing $l = |\langle \mathbf{e}_j \rangle|$ along the diagonal is

$$l = (a^2 + b^2 + 2ab\cos\gamma)^{1/2}, \tag{15}$$

and the angles between the mean axis and the **a** and **b** axes (see Fig. 4*b*) are given by

$$\begin{aligned} \sin\gamma_1 &= b\sin\gamma/l, \\ \sin\gamma_2 &= a\sin\gamma/l. \end{aligned} \tag{16}$$

To derive the statistics of the $\mathbf{e}_j$, the statistics of each primary paracrystal are written in the rotated (by $-\gamma_1$ and γ_2) coordinate systems (using the results of §2.1) and then, since the two primary paracrystals are independent, the variances and covariances can be added to determine the corresponding values for the diagonal paracrystal. The calculation is tedious but straightforward, giving

$$\sigma_e^2 = \sigma_a^2 + \sigma_b^2 + [a^2(\sigma_{b\perp}^2 - \sigma_b^2) + b^2(\sigma_{a\perp}^2 - \sigma_a^2)]\sin^2\gamma/l^2 + p \tag{17}$$

and

$$\sigma_{e\perp}^2 = \sigma_{a\perp}^2 + \sigma_{b\perp}^2 + [b^2(\sigma_a^2 - \sigma_{a\perp}^2) + a^2(\sigma_b^2 - \sigma_{b\perp}^2)]\sin^2\gamma/l^2 - p \tag{18}$$

where

$$p = 2[ab(C_a - C_b) + (b^2C_a - a^2C_b)\cos\gamma]\sin^2\gamma/l^2 \tag{19}$$

and

$$\begin{aligned} C_e = \{&ab(\sigma_{a\perp}^2 - \sigma_a^2 + \sigma_b^2 - \sigma_{b\perp}^2) \\ &+ [b^2(\sigma_{a\perp}^2 - \sigma_a^2) + a^2(\sigma_b^2 - \sigma_{b\perp}^2)]\cos\gamma\} \\ &+ C_a + C_b - 2(b^2C_a + a^2C_b)\sin^2\gamma/l^2. \end{aligned} \tag{20}$$

The implications of these equations are difficult to assess in the general case, however we examine some simple cases for square and hexagonal lattices below. Note that adding (17) and (18) shows that

$$\sigma_e^2 + \sigma_{e\perp}^2 = (\sigma_a^2 + \sigma_{a\perp}^2) + (\sigma_b^2 + \sigma_{b\perp}^2), \tag{21}$$

i.e. the 'total' variance along the diagonal is the sum of the total variances along the primary axes. This is a direct result of the ideal paracrystal construction. A result of this is that the variance along the diagonal is always greater than (or equal to) that along any primary axis.

2.3.1. The square ideal paracrystal. Because of the symmetry of the square lattice, we consider the case where the statistics of the two primary one-dimensional paracrystals are the same. We therefore set $\sigma_a = \sigma_b = \sigma$ and $\sigma_{a\perp} = \sigma_{b\perp} = \sigma_\perp$ and consider the three cases $C_a = C_b = C$, $C_a = -C_b = C$ and $C_a = C_b = 0$. Substituting into (17)–(20) shows that, for $C_a = C_b$, and also for $C_a = C_b = 0$,

$$\begin{aligned} \sigma_e^2 &= \sigma^2 + \sigma_\perp^2 \\ \sigma_{e\perp}^2 &= \sigma^2 + \sigma_\perp^2 \\ C_e &= 0, \end{aligned} \tag{22}$$

and, for $C_a = -C_b$,

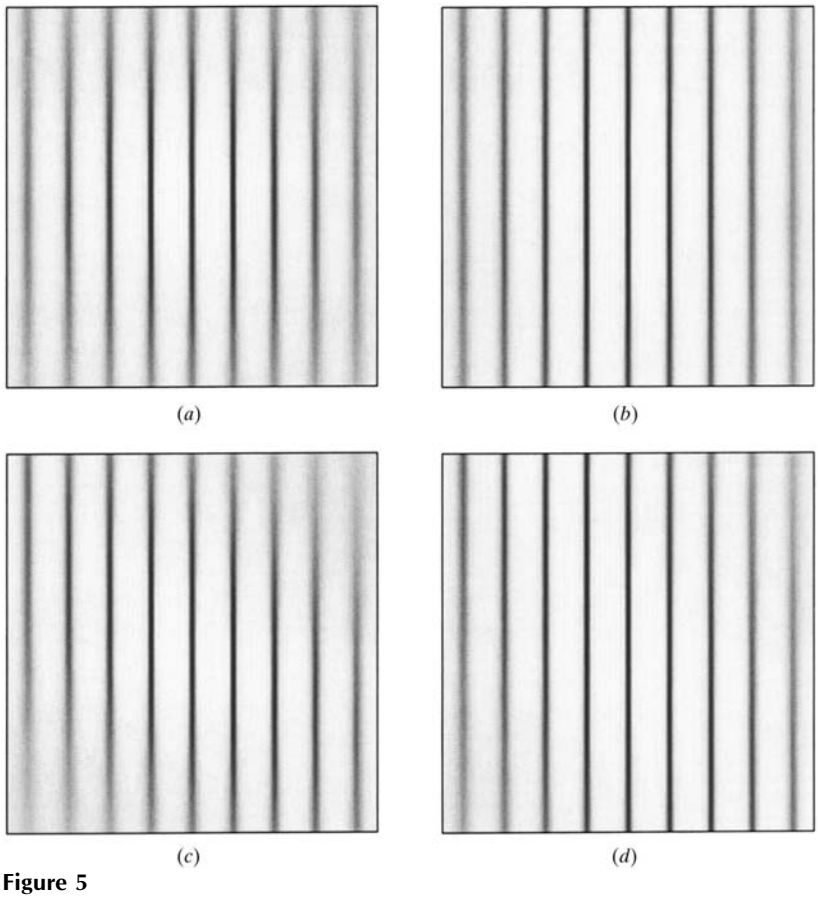

Figure 5
Diffraction patterns from one-dimensional paracrystals in the plane for (*a*) $\sigma_x = \sigma_y = 0.04$, $\rho = 0$; (*b*) $\sigma_x = 0.04$, $\sigma_y = 0.02$, $\rho = 0$; (*c*) $\sigma_x = \sigma_y = 0.04$, $\rho = 0.5$; and (*d*) $\sigma_x = 0.04$, $\sigma_y = 0.02$, $\rho = 0.5$.

$$\begin{aligned}\sigma_e^2 &= \sigma^2 + \sigma_\perp^2 + 2C\\ \sigma_{e\perp}^2 &= \sigma^2 + \sigma_\perp^2 - 2C\\ C_e &= 0.\end{aligned} \tag{23}$$

The variances parallel and normal to the diagonal are equal in (22) but not in (23). The reason for this can be seen by referring to Fig. 3. If both primary paracrystals are positively (or negatively) correlated, the major axes of the two probability ellipses are parallel and orthogonal to the diagonal, so that the net effect is equal in the two directions. If the correlations have opposite signs, the directions of preferential distortion are parallel and they contribute preferentially to the parallel or normal components. In all cases, the parallel and normal components are uncorrelated since correlations in the primary paracrystals give preferential distortions either along the (1, 1) or (1, −1) diagonals. As noted above, in all cases the total variance is equal to the sum of the variances of the primary paracrystals.

2.3.2. The hexagonal ideal paracrystal. Hexagonal lattices are common in crystals of molecules or assemblies that are approximately circular in cross section. Examples include rod-like assemblies, fibrous materials, muscle proteins, biopolymers such as nucleic acids and some synthetic polymers. Disordered packing is not uncommon in such systems (Millane & Stroud, 1991). Since the average spacing along the (1, 1) diagonal is identical to the spacings along the primary axes for hexagonal lattices, intermolecular interactions may be similar for approximately circular molecules and the statistics along the diagonal are particularly relevant. Owing to the hexagonal symmetry, we consider the case where the statistics of the one-dimensional paracrystals along the primary axes are the same, and σ^2, $\sigma_\perp^2$ and C are defined as above. The statistics along the diagonal can then be calculated using (17)–(20), giving, for the case $C_a = C_b$:

$$\begin{aligned}\sigma_e^2 &= \sigma^2/2 + 3\sigma_\perp^2/2\\ \sigma_{e\perp}^2 &= 3\sigma^2/2 + \sigma_\perp^2/2\\ C_e &= -C,\end{aligned} \tag{24}$$

for the case $C_a = -C_b$:

$$\begin{aligned}\sigma_e^2 &= \sigma^2/2 + 3\sigma_\perp^2/2 + 3^{1/2}C\\ \sigma_{e\perp}^2 &= 3\sigma^2/2 + \sigma_\perp^2/2 - 3^{1/2}C\\ C_e &= 0,\end{aligned} \tag{25}$$

and for $C_a = C_b = 0$:

$$\begin{aligned}\sigma_e^2 &= \sigma^2/2 + 3\sigma_\perp^2/2\\ \sigma_{e\perp}^2 &= 3\sigma^2/2 + \sigma_\perp^2/2\\ C_e &= 0.\end{aligned} \tag{26}$$

As with the square lattice, the above results can be interpreted in terms of rotated copies of the probability ellipses shown in Fig. 3.

Inspection of (24)–(26) shows that, as anticipated, it is not possible to choose the disorder parameters such that the disorder along the diagonal is identical to the disorder along the primary axes, *i.e.* the disorder does not have hexagonal symmetry. This is particularly troublesome for the hexagonal lattice since the average lattice spacing along the diagonal is the same as along the primary axes, so that, for molecules with circular or hexagonal cross sections, similar contacts, and therefore similar disorder, would be expected along these directions. The ideal paracrystal is therefore probably not a suitable model of disorder in such systems. It may be possible to devise disordered lattice models that have the required symmetry, but they would not be ideal paracrystals. One such model is that of Busson & Doucet (2000), although the statistics of the individual lattices are not defined in that model.

3. Diffraction by the ideal paracrystal

The diffraction pattern from an ideal paracrystalline lattice is easily derived in terms of the diffraction from a one-dimensional paracrystal. The diffraction from a one-dimensional lattice of N sites in the plane is given by

$$F_1(u, v) = \sum_{j=0}^{N-1} \exp(i2\pi[ux_j + vy_j]), \tag{27}$$

where the subscript 1 indicates a one-dimensional paracrystal and (u, v) are Cartesian coordinates in reciprocal space. The intensity diffracted by a collection of such lattices is given by the intensity averaged over all realizations of the lattice, *i.e.*

$$\begin{aligned}I_1(u, v) &= \langle |F_1(u, v)|^2 \rangle\\ &= \sum_{j=0}^{N-1}\sum_{k=0}^{N-1} \langle \exp(i2\pi[u(x_j - x_k) + v(y_j - y_k)]) \rangle.\end{aligned} \tag{28}$$

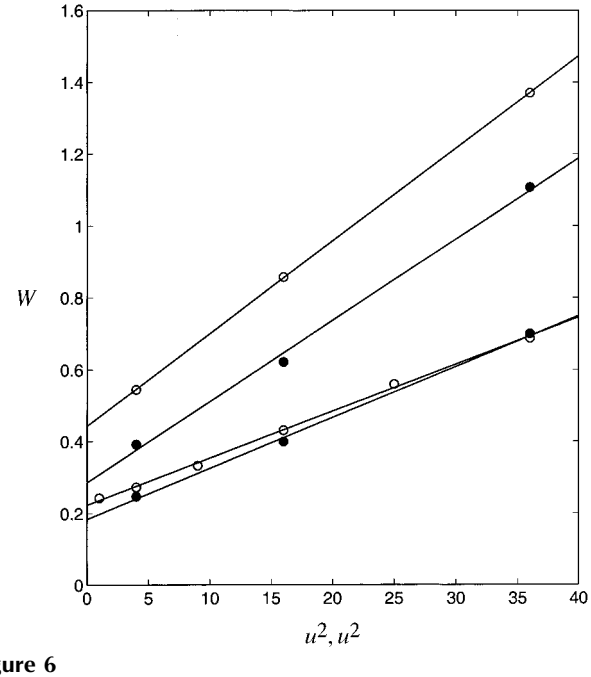

Figure 6
Peak widths (W) for one-dimensional (Fig. 5*a*) (open circles) and two-dimensional (Fig. 9*a*) (filled circles) paracrystals as described in the text. For each set, the lower curve is the width in u plotted *versus* u^2, and the upper curve is the width in w *versus* w^2.

Since $\langle x_j \rangle = ja$, (28) can be written as

$$I_1(u, v) = \sum_{j=0}^{N-1} \sum_{k=0}^{N-1} \exp(i2\pi ua[j-k]) \times \langle \exp(i2\pi[(u\xi_j + vy_j) - (u\xi_k + vy_k)]) \rangle, \quad (29)$$

where $\xi_j = x_j - ja$. The ξ_j and y_j are zero-mean normally distributed random variables with variances σ_x^2 and σ_y^2, respectively, and covariance C. The average in (29) can therefore be evaluated and the double sum reduced to a single sum as for the case of a one-dimensional paracrystal on a line [see, for example, Appendix A of Millane & Eads (2000) for details], giving

$$I_1(u, v) = N + 2 \sum_{j=1}^{N-1} (N-j) \cos(2\pi uaj) \times \exp(-2\pi^2[\sigma_x^2 u^2 + 2Cuv + \sigma_y^2 v^2] j). \quad (30)$$

From (11) and using the convolution theorem used for Fourier transforms, one has that the diffraction from the ideal paracrystal is given by

$$G(u, v) = F_a(u, v) F_b(u, v), \quad (31)$$

where the subscripts denote the one-dimensional paracrystals along the a and b directions. The intensity diffracted by a collection of ideal paracrystals is therefore given by

$$\begin{aligned} I(u, v) &= \langle |G(u, v)|^2 \rangle \\ &= \langle |F_a(u, v)|^2 |F_b(u, v)|^2 \rangle \\ &= I_a(u, v) I_b(u, v), \end{aligned} \quad (32)$$

since the two one-dimensional paracrystals are independent. Taking the two one-dimensional paracrystals to be oriented as in §2.2, the diffraction pattern $I_b(u, v)$ is rotated by γ, so that

$$I(u, v) = I_1(u, v) I_1(u \cos\gamma + v \sin\gamma, -u \sin\gamma + v \cos\gamma). \quad (33)$$

The intensity diffracted by a collection of finite two-dimensional ideal paracrystals can therefore be calculated using (30) and (33).

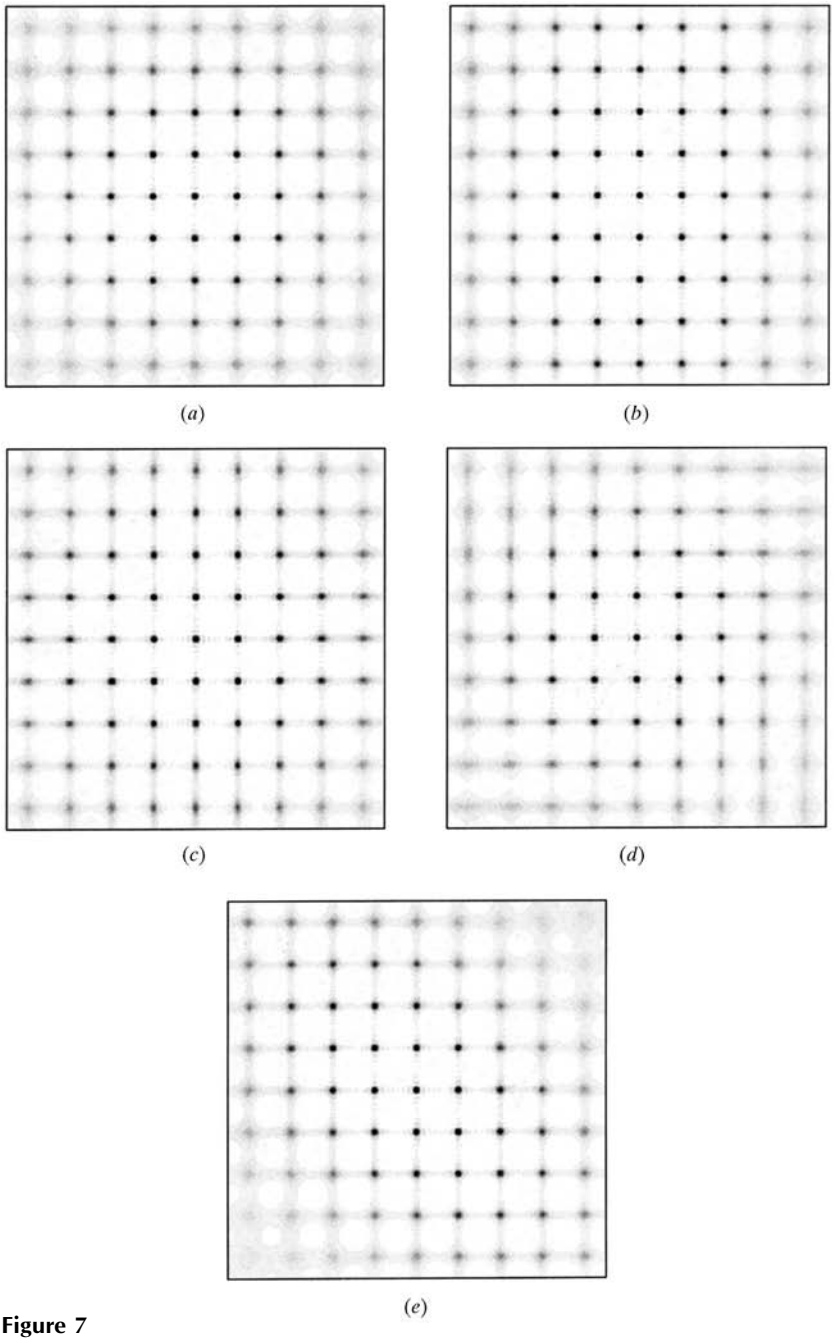

Figure 7
Diffraction patterns from two-dimensional square ideal paracrystals for (*a*) $\sigma_a = \sigma_{a\perp} = \sigma_b = \sigma_{b\perp} = 0.04$, $\rho_a = \rho_b = 0$; (*b*) $\sigma_a = \sigma_{b\perp} = 0.04$, $\sigma_{a\perp} = \sigma_b = 0.02$, $\rho_a = \rho_b = 0$; (*c*) $\sigma_a = \sigma_b = 0.04$, $\sigma_{a\perp} = \sigma_{b\perp} = 0.02$, $\rho_a = \rho_b = 0$; (*d*) $\sigma_a = \sigma_{a\perp} = \sigma_b = \sigma_{b\perp} = 0.04$, $\rho_a = \rho_b = 0.5$; and (*e*) $\sigma_a = \sigma_{a\perp} = \sigma_b = \sigma_{b\perp} = 0.04$, $\rho_a = 0.5$, $\rho_b = -0.5$.

4. Examples of diffraction patterns

4.1. The one-dimensional paracrystal

Since the diffraction pattern from an ideal paracrystal is equal to the product of the diffraction patterns from two one-dimensional paracrystals, it is instructive to first consider the latter diffraction patterns. Examples of diffraction patterns from one-dimensional paracrystals in the plane ($N = 8$, $a = 1$) are shown in Fig. 5. All diffraction patterns are shown on the interval $-4.5 < u < 4.5$, $-4.5 < v < 4.5$, with the u and v axes horizontal and vertical, respectively. The parameters of the paracrystals are given in the figure captions. Since the lattices are one-dimensional, the diffraction patterns contain bands of intensity and, as a result of the cumulative disorder, the width of the bands increases with increasing u and v (Fig. 5*a*). For $\sigma_x > \sigma_y$, the width of the bands increases more rapidly with u than with v (Fig. 5*b*). For $\sigma_x = \sigma_y$ and $\rho > 0$, the largest distortions of the lattice sites occur for distortions at 45° to the x axis

(see Fig. 3), and the width of the bands in the diffraction pattern consequently increases most rapidly along the corresponding direction in reciprocal space (Fig. 5*c*). For $\sigma_x \neq \sigma_y$ and $\rho \neq 0$, the widths of the bands in the diffraction pattern increase most rapidly in the direction corresponding to the orientation of the major axis of the probability ellipse as shown in Fig. 3 (Fig. 5*d*).

As mentioned above, an important application of the paracrystalline model is the estimation of distortion parameters from an analysis of peak widths *versus* scattering angle. It is therefore useful to examine the variation of the peak widths on the diffraction patterns in Fig. 5 along particular directions in reciprocal space. For the one-dimensional paracrystal (on a line), the peak width (integral breadth or the area under the peak divided by its height, both above the background), W, increases with increasing scattering angle, and for low-order reflections approximately follows the relationship (Guinier, 1963; Hosemann & Hindeleh, 1995)

$$W = l^{-1} + \pi^2 a \sigma^2 u^2, \tag{34}$$

where $l = aN$ is the mean crystallite length. Therefore, plots of W *versus* u^2 are approximately linear and allow l and σ^2 to be estimated from the intercept and slope, respectively. For a reflection whose profile is approximately Gaussian, it is easy to show that the integral breadth is 2.1 times the full width at half-maximum (FWHM).

For a one-dimensional paracrystal in the plane, referring to (30) shows that the diffraction pattern on the u axis is identical to that from a one-dimensional paracrystal on a line with variance σ_x^2 (*i.e.* the diffraction is independent of σ_y and ρ). A plot of the widths W (calculated from the FWHM as described above) of the bands in Fig. 5(*a*) measured along the u axis, *versus* u^2, is shown in Fig. 6 (lower set of open circles). The points fit a straight line and measurement of the slope and intercept gives $\sigma = 0.037$ and $l = 5$, compared to the actual values of 0.04 and 7.

When examining peak widths in diffraction patterns from hexagonal ideal paracrystals later, the widths of the bands in Fig. 5 along lines at $\pm 60^\circ$ to the u axis will be relevant. We examine these widths for the case $\sigma_x = \sigma_y$ and no correlations (Fig. 5*a*). Let w denote distance along the line at 60° to the u axis in Fig. 5(*a*). The equation of this line is $v = 3^{1/2}u$ and $w = 2u$, so that, referring to (30), the intensity $I_{1w}(w)$ along this line is given by

$$\begin{aligned} I_{1w}(w) &= I_1\left(\frac{w}{2}, \frac{3^{1/2}w}{2}\right) \\ &= N + 2\sum_{j=1}^{N-1}(N-j)\cos(\pi w a j) \\ &\quad \times \exp(-2\pi^2\sigma^2 w^2 j). \end{aligned} \tag{35}$$

Referring to (30) also shows that

$$\begin{aligned} I_1(u,0) &= N + 2\sum_{j=1}^{N-1}(N-j)\cos(2\pi u a j) \\ &\quad \times \exp(-2\pi^2\sigma^2 u^2 j). \end{aligned} \tag{36}$$

The peaks in $I_{1w}(w)$ occur at $w = 2m/a$, and the peaks in $I_1(u, 0)$ occur at $u = m/a$, where m is an integer. Inspection of (35) and (36) shows that the exponential factors are slowly varying functions, and that the behavior of the diffraction in the vicinity of a peak is determined by the cosine factors. In the vicinity of the point $w = 2m/a$, the arguments of the cosine factors in (35) are $(2\pi mj)$, and in the vicinity of the point $u = 2m/a$ (*i.e.* every second peak along the u axis), the arguments of the cosine factors in (36) are $(4\pi mj)$, and the exponential factors are identical. Therefore, the peak widths of $I_{1w}(w)$ are twice those of $I_1(u, 0)$ where $w = u$. The peak widths along the line at 60° to the u axis on the diffraction pattern shown in Fig. 5(*a*) were measured and are plotted in Fig. 6 *versus* w^2 (upper set of open circles). These widths are, in fact, exactly twice those of the corresponding peaks on the u axis (lower set of open circles).

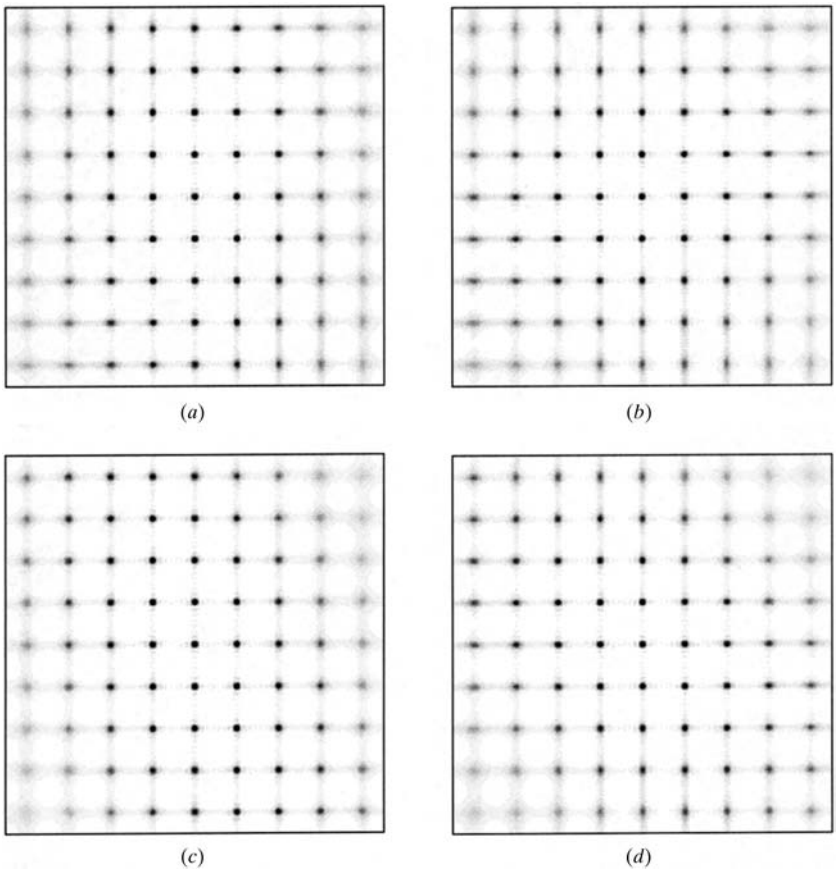

Figure 8
Diffraction patterns from two-dimensional square ideal paracrystals with correlations and unequal variances, for (*a*) $\sigma_a = \sigma_{b\perp} = 0.04$, $\sigma_{a\perp} = \sigma_b = 0.02$, $\rho_a = \rho_b = 0.5$; (*b*) $\sigma_a = \sigma_b = 0.04$, $\sigma_{a\perp} = \sigma_{b\perp} = 0.02$, $\rho_a = \rho_b = 0.5$; (*c*) $\sigma_a = \sigma_{b\perp} = 0.04$, $\sigma_{a\perp} = \sigma_b = 0.02$, $\rho_a = 0.5$, $\rho_b = -0.5$; and (*d*) $\sigma_a = \sigma_b = 0.04$, $\sigma_{a\perp} = \sigma_{b\perp} = 0.02$, $\rho_a = 0.5$, $\rho_b = -0.5$

4.2. The ideal paracrystal

Characteristics of diffraction patterns from two-dimensional ideal paracrystals are explored by calculation using (33) for square and hexagonal lattices to show the effects of the different parameters. The characteristics of the diffraction patterns are discussed for the square lattice and the peak widths are discussed for the hexagonal lattice. An 8×8 site lattice with unity average lattice spacing ($a = 1$) is used for all the examples. All of the diffraction patterns can be interpreted in terms of two rotated distributions (of the kind shown in Fig. 3) and multiplication of the two corresponding diffraction patterns from one-dimensional paracrystals.

Diffraction patterns from square ideal paracrystals are shown in Figs. 7 and 8. For $\sigma_a = \sigma_{a\perp} = \sigma_b = \sigma_{b\perp}$ and no correlations (Fig. 7*a*), the diffraction spots streak along the two reciprocal-space axes, which is a result of the anisotropic nature of the ideal paracrystal model. If $\sigma_{a\perp}$ and σ_b are decreased, then the major axes of the probability ellipses are both parallel to the x axis and the width of the bands in Fig. 5 increase more rapidly with u. The result (Fig. 7*b*) is that the reflections remain symmetric in u and v but broaden (and hence reduce their peak amplitude) more rapidly in the u direction than in the v direction. If $\sigma_{a\perp}$ and $\sigma_{b\perp}$ are decreased, the major axes of the probability ellipses are orientated along the x and y axes so that the contributing vertical bands (Fig. 5) in the diffraction pattern increase in width more rapidly with u and the widths of the horizontal bands increase more rapidly with v. The result (Fig. 7*c*) is that the reflections are asymmetric in u and v, being wider in the u direction than the v direction for $u > v$ and *vice versa* for $u < v$, and are symmetric only on the lines $u = \pm v$. If both one-dimensional paracrystals are positively correlated (for equal variances), the width of the reflections in the u direction increases most rapidly along a line at 45° to the u axis and the width in the v direction increases most rapidly along a line at −45° to the u axis. The result is that the reflections are most asymmetric along lines inclined at ±45° to the u axis and are symmetric along the u and v axes (Fig. 7*d*), giving the overall pattern a spiral appearance. For opposite correlations, the u widths of the vertical bands and the v widths of the horizontal bands both increase most rapidly along the line at 45° to the u axis, and the two components increase at the same rate in all directions. The result is that all the reflections are symmetric in u and v, and the peak amplitudes reduce most rapidly along a line at 45° to the u axis (Fig. 7*e*).

Diffraction patterns from ideal paracrystals with unequal variances and with correlations are shown in Fig. 8. Cases for equal correlations are shown in Figs. 8(*a*) and 8(*b*), and opposite correlations in Figs. 8(*c*) and 8(*d*). For equal correlations with σ_a and $\sigma_{b\perp}$ greater than $\sigma_{a\perp}$ and σ_b (Fig. 8*a*), the two contributing probability ellipses (Fig. 3) have their major axes oriented at $\sim \pm 20°$ to the x axis. The result is that the u widths and the v widths of

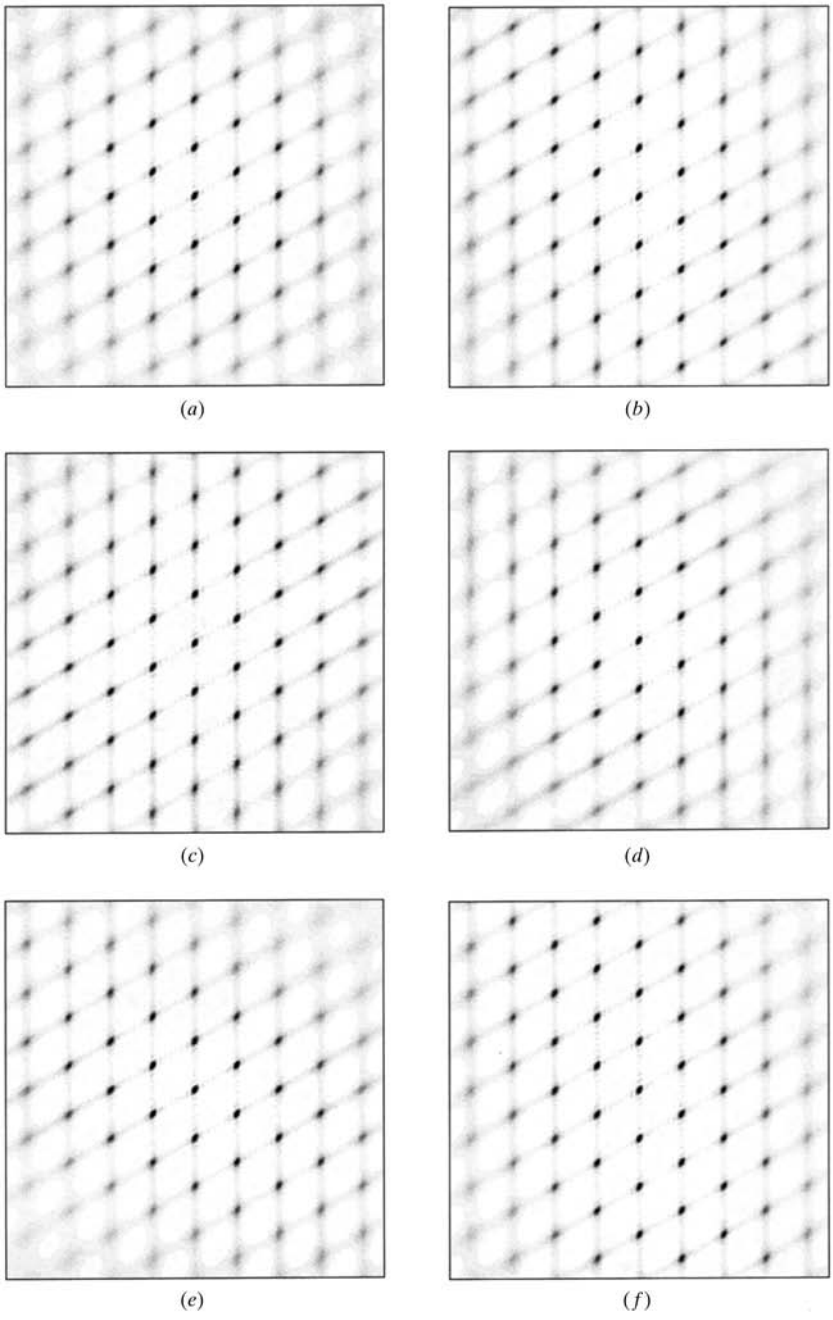

Figure 9
Diffraction patterns from two-dimensional hexagonal ideal paracrystals for (*a*) $\sigma_a = \sigma_{a\perp} = \sigma_b = \sigma_{b\perp} = 0.04$, $\rho_a = \rho_b = 0$; (*b*) $\sigma_a = \sigma_{b\perp} = 0.04$, $\sigma_{a\perp} = \sigma_b = 0.02$, $\rho_a = \rho_b = 0$; (*c*) $\sigma_a = \sigma_b = 0.04$, $\sigma_{a\perp} = \sigma_{b\perp} = 0.02$, $\rho_a = \rho_b = 0$; (*d*) $\sigma_a = \sigma_{a\perp} = \sigma_b = \sigma_{b\perp} = 0.04$, $\rho_a = \rho_b = 0.5$; (*e*) $\sigma_a = \sigma_{a\perp} = \sigma_b = \sigma_{b\perp} = 0.04$, $\rho_a = 0.5$, $\rho_b = -0.5$; and (*f*) $\sigma_a = \sigma_{b\perp} = 0.04$, $\sigma_{a\perp} = \sigma_b = 0.02$, $\rho_a = \rho_b = 0.5$.

the reflections increase most rapidly (and the peak amplitudes decrease rapidly) along lines oriented at ~ 20 and $\sim -20^\circ$, respectively, to the u axis. The reflections are symmetric in u and v along the u and v axes and asymmetric elsewhere, and the overall amplitude of the pattern falls off more rapidly with increasing u than with increasing v. For the case σ_a and σ_b greater than $\sigma_{a\perp}$ and $\sigma_{b\perp}$ (Fig. 8*b*), the major axes of the two probability ellipses are oriented at ~ 20 and $\sim -70^\circ$ to the x axis. The result is that the u widths and the v widths of the reflections increase most rapidly along lines oriented at ~ 20 and $\sim -70^\circ$, respectively, to the u axis, and reflections are symmetric along the orthogonal directions. Since the two probability ellipses are orthogonal, the overall amplitude of the pattern is approximately circularly symmetric. For opposite correlations with σ_a and $\sigma_{b\perp}$ greater than $\sigma_{a\perp}$ and σ_b (Fig. 8*c*), the major axes of the two probability ellipses are both oriented at $\sim -20^\circ$ to the x axis. The u and v widths of the reflections then both increase at the same rate in any particular direction in reciprocal space, so that *all* the reflections are symmetric in u and v, and broaden most rapidly in the direction at $\sim 20^\circ$ to the u axis. For opposite correlations with σ_a and σ_b greater than $\sigma_{a\perp}$ and $\sigma_{b\perp}$ (Fig. 8*d*), the major axes of the two probability ellipses are oriented at ~ 20 and $\sim 70^\circ$ to the x axis. The u width and v width of the reflections then increase most rapidly along lines oriented at 20 and 70°, respectively, to the u axis, the reflections are symmetric in u and v along lines at $\pm 45^\circ$ to the u axis, and the overall amplitude of the pattern falls off most rapidly along a line at 45° to the u axis.

A selection of diffraction patterns for hexagonal ideal paracrystals is shown in Fig. 9. Note that the reflections streak along the a^* (30° to the u axis) and b^* (vertical) directions and, in particular, that the reflections do not have hexagonal symmetry as a result of the anisotropic disorder as discussed earlier. The overall characteristics of these diffraction patterns can be interpreted in the same kind of way as described above for square ideal paracrystals. Since the average spacing along the diagonal direction in real space is equal to that along the primary axes, it is of interest to examine the diffraction along the corresponding directions in reciprocal space, in particular the variation in peak widths. We do this only for the case $\sigma_a = \sigma_{a\perp} = \sigma_b = \sigma_{b\perp} = 0.04$ and $\rho = 0$ (Fig. 9*a*), as the other cases get progressively more complicated. In this case, the profiles along the directions parallel to a and b are identical, but those along the direction parallel to the diagonal are broader, as shown in Fig. 10. The diffraction pattern in Fig. 9(*a*) is equal to the product of the pattern in Fig. 5(*a*) with itself rotated by 120°. The diffracted intensity along the u axis (*i.e.* parallel to a) is then given by

$$I(u, 0) = I_1(u, 0) I_{1w}(u) \tag{37}$$

and the intensity along the w axis (*i.e.* parallel to the cell diagonal), $I_w(w)$, by

$$I_w(w) = [I_{1w}(w)]^2. \tag{38}$$

Since peaks in the diffraction pattern from the ideal paracrystal occur only where the bands in the patterns from the two one-dimensional paracrystals overlap, the reflection profiles in the former are the products of the relevant profiles in the latter. For two profiles that are approximately Gaussian with widths W_1 and W_2, their product is approximately Gaussian with width $W_1 W_2/(W_1^2 + W_2^2)^{1/2}$. As shown in §4.1, the peak widths of $I_{1w}(w)$ are twice those of $I_1(u, 0)$, and therefore the peak widths of $I(u, 0)$ should be $2/5^{1/2} \approx 0.9$ times those of $I_1(u, 0)$, and the peak widths of $I_w(w)$ should be $2^{1/2} \approx 1.4$ times those of $I_1(u, 0)$. The corresponding peak widths in Fig. 9(*a*) were measured and are plotted in Fig. 6 (filled circles). The ratios of the measured peak widths of $I(u, 0)$ and $I_w(w)$ to those of $I_1(u, 0)$ vary in the ranges 0.9–1.0 and 1.4–1.6, respectively, showing good agreement with the above analysis. From (26), the parallel standard deviation of the chain along the x axis is 0.040 and the parallel standard deviation of the chain along the diagonal is $0.04 \times 2^{1/2} \approx 0.057$. Calculation of these parameters from the slopes of the plots in Fig. 6 gives 0.038 and 0.048, which are reasonably good estimates of the actual values.

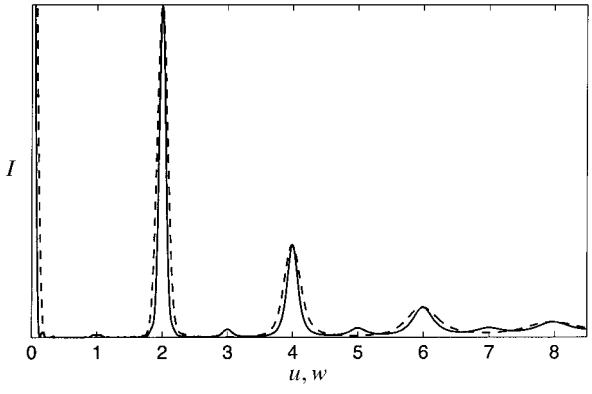

Figure 10
Plots of the diffracted intensity in Fig. 9(*a*) along the lines parallel to a and b (solid line) and along the line parallel to the cell diagonal in real space (dashed line).

5. Conclusions

The ideal paracrystal is the only direct generalization of the one-dimensional paracrystal to two dimensions for which the statistics are well defined and the diffraction easily calculated. The statistics of the general, finite, two-dimensional ideal paracrystal have been described and expressions for diffraction patterns derived. Computed diffraction patterns show a wide variety of characteristics and interpretation of such patterns in terms of parameters of the ideal paracrystal is not straightforward. The above results indicate that reasonably good estimates of parallel variances can be obtained by interpreting peak broadening in terms of a one-dimensional model. However, the lack of hexagonal symmetry in the disorder for hexagonal lattices indicates limited utility of the model in this case.

We are grateful to the US National Science Foundation for support (DBI-9722862).

References

Alexander, L. E. (1969). *X-ray Diffraction Methods in Polymer Science*, ch. 7. Malabar, FL: Robert E. Krieger.

Baltá-Calleja, F. J. & Hosemann, R. (1980). *J. Appl. Cryst.* **13**, 521–523.

Biswas, A. & Blackwell, J. (1988). *Macromolecules*, **21**, 3146–3151.

Brämer, R. & Ruland, W. (1976). *Makromol. Chem.* **177**, 3601–3617.

Busson, B. & Doucet, J. (2000). *Acta Cryst.* A**56**, 68–72.

Eads, J. L. & Millane, R. P. (2000). *Acta Cryst.* A**56**, 549–553.

Egelman, E. H. & DeRosier, D. J. (1982). *Acta Cryst.* A**38**, 796–799.

Granier, T., Thomas, E. & Karasz, F. (1989). *J. Polym. Sci. Part B: Polym. Phys.* **27**, 469–487.

Guinier, A. (1963). *X-ray Diffraction in Crystals, Imperfect Crystals and Amorphous Bodies.* New York: W. H. Freeman.

Hall, I. H. & Somashekar, R. (1991). *J. Appl. Cryst.* **24**, 1051–1059.

Hammersley, J. M. (1967). *Proc. 5th Berkeley Symp. on Mathematical Statistics and Probability*, Vol. 3, pp. 89–118. Berkeley: University of California Press.

Hosemann, R. & Bagchi, S. (1962). *Direct Analysis of Diffraction by Matter.* Amsterdam: North-Holland.

Hosemann, R. & Hindeleh, A. (1995). *J. Macromol. Sci. Phys.* B**34**, 327–356.

Hosemann, R. & Müller, B. (1970). *Mol. Cryst. Liquid Cryst.* **10**, 273–294.

Hosemann, R., Vogel, W., Weick, D. & Baltá-Calleja, F. J. (1981). *Acta Cryst.* A**37**, 85–91.

Janke, M. & Hosemann, R. (1978). *Prog. Colloid Polym. Sci.* **64**, 226–231.

Matsuoka, H., Tanaka, H., Hashimoto, T. & Ise, N. (1987). *Phys. Rev. B*, **36**, 1754–1765.

Millane, R. P. & Eads, J. L. (2000). *Acta Cryst.* A**56**, 497–506.

Millane, R. P. & Stroud, W. J. (1991). *Int. J. Biol. Macromol.* **13**, 202–208.

Mu, X. Q., Makowski, L. & Fairchild, B. M. (1997). *Acta Cryst.* A**53**, 55–62.

Perret, R. & Ruland, W. (1971). *Kolloid Z. Z. Polym.* **247**, 835.

Stroud, W. J. & Millane, R. P. (1995). *Acta Cryst.* A**51**, 790–800.

Stroud, W. J. & Millane, R. P. (1996). *Proc. R. Soc. London Ser. A*, **452**, 151–173.

Welberry, T. R. (1985). *Rep. Prog. Phys.* **48**, 1543–1593.

Welberry, T. R. & Butler, B. D. (1995). *Chem. Rev.* **95**, 2369–2403.

Welberry, T. R. & Carroll, C. E. (1982). *Acta Cryst.* A**38**, 761–772.

Welberry, T. R., Miller, G. H. & Carroll, C. E. (1980). *Acta Cryst.* A**36**, 921–929.